Multiple bound states in sharply bent waveguides

John P. Carini
Department of Physics, Indiana University, Bloomington, Indiana 47405

J. T. Londergan
Department of Physics, Indiana University, Bloomington, Indiana 47405
and Nuclear Theory Center, Indiana University, 2401 Milo Sampson Lane, Bloomington, Indiana 47408-0768

Kieran Mullen
Department of Physics, Indiana University, Bloomington, Indiana 47405

D. P. Murdock
Nuclear Theory Center, Indiana University, 2401 Milo Sampson Lane, Bloomington, Indiana 47408-0768
and Department of Physics, Tennessee Technological University, Cookeville, Tennessee 38505
(Received 17 March 1993)

We present experimental and theoretical results on bound states in rectangular bent waveguides. Such bound states can be observed in electromagnetic waveguides and quantum wires. For a class of bent waveguides one can produce confined TE modes; such TE modes are directly related to bound states of scalar fields in the curved two-dimensional space from which the waveguides are constructed. For sufficently sharp bends, one can produce multiple bound TE modes. We calculate the bound-state energies and field configurations for a particular class of sharply bent waveguides. These waveguides are constructed, and both bound-state energies and fields are directly measured and compared with theoretical predictions.

I. INTRODUCTION

The properties of electromagnetic fields in waveguides have been studied for decades.[1] Many features of the nature and transmission of em fields in waveguides have long been understood. One well-known fact is that bends in waveguides produce reflection, and that reflection resonances can arise when bends are introduced into waveguides. To the best of our knowledge, it has only recently been realized that the introduction of bends into waveguides generally leads to *confined* states, or isolated modes which exist below the cutoff frequency for the waveguide. In such confined states, the E and B fields are large in the region of the bend and fall off exponentially down the length of the waveguide.

Such confined states are interesting not only for their intrinsic applications to electromagnetic waveguides, but also for their analogs in quantum wires. It is possible to make a correspondence between solutions of the three-dimensional Maxwell equations in a waveguide and the two-dimensional Schrödinger equation in a quantum channel or wire.[2-8] By understanding the properties of the former, we can gain information about the latter.

In this paper we shall examine bent waveguides which support several bound states. Since the binding energy of the lowest state, and the number of bound states which can exist in a bent waveguide, depends upon the size of the bend and/or the existence of "extra" space in the bend, we will review the conditions for bound states in bent waveguides. We will examine this question from both theoretical and experimental perspectives; we will calculate energies and fields for such states in bent waveguides, construct such waveguides, and compare their experimental properties with theoretical predictions.

We begin by reviewing the properties of bound states for scalar fields satisfying the Helmholtz equation in two dimensions, as our understanding of the existence and properties of such states arose from the relation between two-dimensional systems and TE modes in waveguides constructed from such systems. To understand this connection, consider a rectangular waveguide constructed in the following way (we repeat the argument of Goldstone and Jaffe[9]). Produce some two-dimensional surface σ in the x-y plane, with surface boundary $\mathcal{S}$, shown schematically in Fig. 1(a). Then translate this surface normally in the z direction, as shown in Fig. 1(b), to produce the three-dimensional region $\mathcal{D}$. If a scalar field $\psi(x,y)$ defined on σ satisfies the conditions

$$[\nabla^2+k^2]\psi(x,y)=0 \quad (x,y)\in\sigma \ , \qquad \psi(x,y)|_{\mathcal{S}}=0 \ , \tag{1}$$

then E and B fields of the form $\mathbf{E}=ik\psi\hat{\mathbf{z}}$, $\mathbf{B}=-\hat{\mathbf{z}}\times\nabla\psi$ will satisfy Maxwell's equations and the boundary conditions for TE modes in this waveguide.

Thus for any two-dimensional surface σ containing a scalar field ψ which obeys the Helmholtz equation inside σ and vanishes on the boundary, one can straightforwardly construct TE em fields for the rectangular waveguide constructed from σ. Recently it has been proven that a large class of such two-dimensional sur-

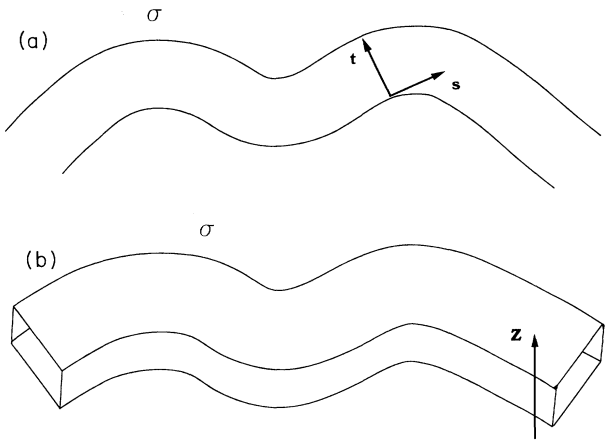

FIG. 1. (a) The infinitely long curved two-dimensional surface σ; the surface is in the x-y plane, with curvilinear coordinates s along the surface and t normal to the surface at each point. (b) The rectangular waveguide constructed from the surface σ of part (a) by extending the surface upward in the z direction.

faces, with solutions satisfying the conditions of Eq. (1), possess bound states.[2,3,9–12] Consequently, the corresponding waveguides have at least one TE mode which is confined in space; such fields exist below the cutoff frequency for the waveguide, and they fall off exponentially like the scalar fields from which they are derived.

To review the properties of two-dimensional systems which possess bound states, consider a curved surface σ of constant width and infinite length, as shown in Fig. 1(a). Eventually the surface becomes straight with constant width, but it can curve arbitrarily in the middle. The surface has no potential on the inside but the wave function is required to vanish on the surface (the equivalent of infinite potential walls at the edge of the surface). Goldstone and Jaffe[9] proved that all such surfaces possess at least one bound state, except for the surface which is straight everywhere. This result is surprising: since such surfaces have no "classically forbidden" region (there is nothing to prevent a classical particle from moving down the tube), it is not obvious why such systems should have any bound states; the fact that at least one bound state exists for a tube of constant width with a bend *anywhere* is quite unexpected. In these two-dimensional systems, bound states do not arise from the "traditional" picture, where a binding potential creates classically allowed and forbidden regions. Here the boundary conditions (vanishing of the wave function on the waveguide boundaries) give an effective confining potential which produces a minimum (cutoff) energy for continuum solutions (bands of propagating states).

The easiest system to analyze is an "L-shaped" tube of infinite length, with a right-angle bend in the middle (although this tube does not in fact have constant width, it still possesses a bound state; we shall return to this point). Lenz *et al.*[10] first noticed the presence of a bound state in such a system, in developing models where confinement and scattering in multiquark systems were reformulated as a two-dimensional scattering problem. Schult, Ravenhall, and Wyld[11] independently derived this result and pointed out potential applications to "quantum wires," narrow two-dimensional substrates in condensed matter physics which allow electrons to propagate in the channels formed by these surfaces, but require their wave functions to vanish on the surfaces. Such systems have been used extensively to study quantum interference effects. The relevance of bound states in such systems, and the possible applications arising from them, have been discussed at length.[4–7,13,14] Exner and coworkers[2,3] proved that large classes of two-dimensional surfaces of constant width possessed bound states, and Goldstone and Jaffe[9] derived a significantly more general result, and also extended this result to an infinite tube of constant cross section in any number of dimensions. Sols and Macucci[7] investigated the properties of bound states in curved wires. Dunne and Jaffe[12] have shown that similar results can be obtained for a tube threaded by an Aharonov-Bohm[15] flux line, namely that such a system possesses a bound state unless the tube is perfectly straight.

In a previous paper,[8] we demonstrated the presence of a bound TE mode for rectangular bent waveguides. Microwaves were pumped into the center of bent waveguides, and the ratio of reflected to incident power was measured there. At the frequency of the confined state, there was a sharp minimum in the reflected power, representing a resonant absorption of the microwave power. The power was actually absorbed by Ohmic heating inside the waveguide bend; since the frequency of this mode was below the lowest cutoff frequency of the waveguide, the electromagnetic fields for the confined state decayed exponentially along the length of the waveguide, and so very little power "leaked out" the open ends of the waveguides even for finite-length waveguides. At other frequencies below cutoff almost 100% of the power was reflected back to the generator. The frequency of the bound states relative to the cutoff frequency of the waveguides agreed very well with theoretical predictions.

The binding energy in such systems goes to zero as the bend angle goes to zero, and binding increases with increasing bend angle. For sufficiently sharp bends, it should be possible to produce multiple bound states. The existence of multiple bound states and their properties is the focus of this paper. The particular geometry we employ is the sharply bent rectangular system shown in Fig. 2(a). We shall show that as the exterior bend angle $\theta_e \rightarrow \pi$, the number of bound states increases dramatically. This occurs both because of the bend, and because there is additional space in the corner of the waveguide (a "bulge" exists in this region). In Sec. II, we show how both bends and bulges produce the effective attraction which produces binding. We review the effective potentials due to bends and bulges in the adiabatic limit, and for sharply bent systems given by Fig. 2(a) we derive upper limits for the energies of bound states as a function of the bend angle.

In Sec. III, we review two numerical methods for cal-

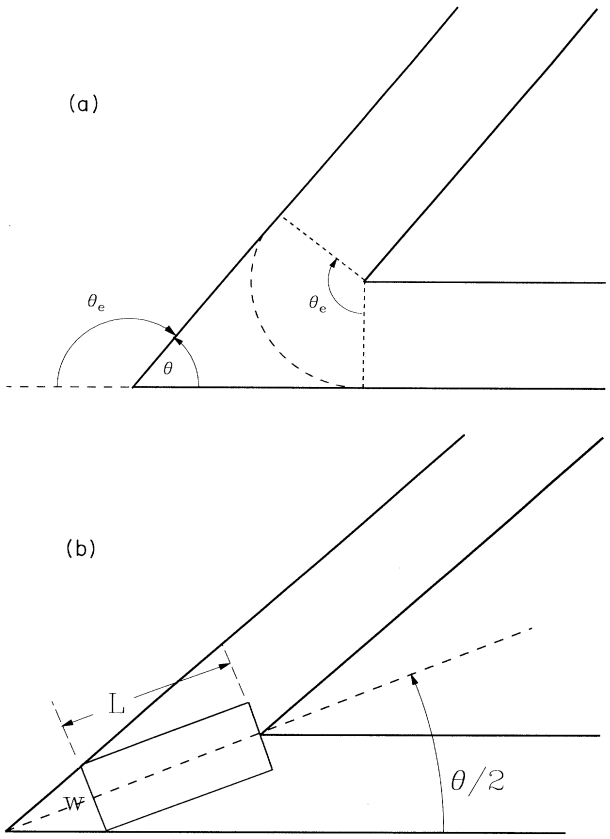

FIG. 2. (a) The sharply bent two-dimensional surface, defined by exterior bend angle θ_e, or equivalently by interior angle $\theta=\pi-\theta_e$. The dashed curve is an arc of the circle of the unit radius and angle θ_e, centered at the interior corner of waveguide. (b) The bent surface of part (a) with an inscribed rectangle of length L and width W.

culating bound-state energies and fields in these waveguides. We used a relaxation method which has been extended to treat states other than the ground state, and we have also used series expansions for the ground-state wave functions. In Sec. IV we discuss the construction of the waveguides, and experimental methods employed to locate the bound states and to map out fields inside the cavities. In Sec. V we give results and discussion, we compare our experimental results with numerical predictions, and we present our conclusions and suggestions for future research in this field.

II. QUALITATIVE DISCUSSION: BOUND STATES IN BENT TWO-DIMENSIONAL SYSTEMS

In this section, we give a qualitative description of bent systems in two dimensions, to present a plausible argument why bends and bulges produce an effective attraction and hence a bound state. First, consider an infinite, bent two-dimensional curve σ of constant width, shown in Fig. 1(a); without loss of generality, normalize the width of the tube to 1. Define curvilinear coordinates s along the tube, and t normal to the length of the tube, with $\kappa(s)$ the curvature of the tube at each point. If $\kappa(s)$ is small and slowly changing, then adiabatically a reasonable trial wave function for the lowest state of the system will be[9]

$$\psi(s,t)\approx\frac{\phi(s)\sin(\pi t)}{\sqrt{1-\kappa(s)t}}\ ;$$

with this approximation the function $\phi(s)$ obeys the differential equation

$$-\frac{d^2\phi}{ds^2}+\{\pi^2-[\kappa(s)]^2/4-k^2\}\phi(s)=0\ . \tag{2}$$

In Eq. (2) the curvature κ gives rise to an effective local attractive potential in the one-dimensional equation satisfied by ϕ. Since any attraction is sufficient to produce a bound state in the one-dimensional Schrödinger equation, any bend will give binding. With the width of the tube normalized to one, the continuum of the system begins at π^2, and an eigenvalue $k^2<\pi^2$ denotes a bound state of the system.

Now take the system of Eq. (2) and make small local changes in the width of the tube: at large distances require that the tube become straight with unit width, in the middle let $W(s)$ denote the width of the tube at point s. If $W(s)$ is always close to 1 and slowly varying, then we can again choose a trial wave function

$$\psi(s,t)\approx\frac{\phi(s)\sin(\pi t/W(s))}{\sqrt{1-\kappa(s)t}}\ ,$$

where $\phi(s)$ obeys the differential equation

$$-\frac{d^2\phi}{ds^2}+\{[\pi/W(s)]^2-[\kappa(s)]^2/4-k^2\}\phi(s)=0\ . \tag{3}$$

Equation (3) again reduces to a one-dimensional differential equation with an effective potential. As before, the curvature κ gives an effective attraction. At very large distances, where the tube is straight with unit width, the overall effective potential tends to π^2. Therefore a bulge or region with $W(s)>1$ constitutes a local attractive potential and a constriction $W(s)<1$ gives an effective repulsion. Since in one dimension any attractive potential will produce a bound state, either a "bulge" or a "bend" is sufficient to produce binding. Equation (3) suggests that a combination of curvature and constriction satisfying $[\pi/W(s)]^2-[\kappa(s)]^2/4=\pi^2$ has zero effective potential (relative to the straight waveguide). Adiabatically, such a system would constitute a completely reflectionless bent waveguide,[16] as the bend and constriction exactly compensate for one another in this limit.

Although the simple arguments given here are valid only for very small bends and changes in width, Goldstone and Jaffe[9] proved that a tube of constant width with *any* bend will support at least one bound state (provided the tube eventually becomes straight). Furthermore, a bent tube which has a bulge (a local increase in width) must also have a bound state. Since the analogous bent tube of constant width has a bound state, the additional space due to the bulge will support a bound state (or states) with lower energy than those for the constant-width tube.

In this paper, we study rectangular waveguides with a sharp bend in the corner, as shown in Fig. 2(a). Such waveguides will have a confined TE mode below cutoff frequency no matter how slight the bend. We can discuss such waveguides in terms of the external bend angle θ_e; it will be more convenient for us to use the supplementary angle $\theta=\pi-\theta_e$, shown in Fig. 2(a), since θ goes to zero as $\theta_e\rightarrow\pi$. We have previously found the confined states for bent waveguides of this type, when $\theta\approx 90°$.[8] In this paper, we will extend our investigations to examine how multiple bound states arise as θ becomes very small.

The energy of the lowest confined state for a bent waveguide decreases monotonically as θ decreases. For sufficiently small values of θ, a second bound state will appear, and more bound states can be found for small enough θ. This can be seen intuitively from the following argument.[17] In the interior of the bend, inscribe a rectangle as shown in Fig. 2(b), and consider the energy eigenvalues for a scalar field which satisfies the Helmholtz equation inside and vanishes on the sides of the rectangle of length L and width W. The energy of such states will be $E_{nm}=\pi^2[n^2/W^2+m^2/L^2]$ for nonzero integer values (n,m). For a bent system with interior angle θ, the length of the inscribed rectangle is related to the width by $L=\csc(\theta/2)[1-W\cos(\theta/2)/2]$. For a given angle θ, we can calculate the dimensions of the inscribed rectangle with the lowest ground-state energy; using these dimensions, we find that as $\theta\rightarrow 0$, the eigenenergies of the box states approach the limiting form

$$E_{nm}\rightarrow\frac{\pi^2}{4}[n^2+(2n^2+m^2)\theta^{2/3}+\cdots]\ . \tag{4}$$

Since the rectangle is inscribed in the waveguide, its eigenenergies provide an upper limit for the energies of the states of the full problem. For every solution of Eq. (4) with an energy below the cutoff for propagation (π^2 in our units), there will be one bound state in the waveguide.

Although the arguments leading to Eq. (4) are very simplistic, the qualitative features agree with detailed calculations described in Secs. III and V. For sufficiently small values of θ, multiple bound states occur. From Eq. (4), the lowest states will have $n=1$ and increasing values of m. The energies of such states have been calculated, and as predicted we find that all bound-state energies approach $\pi^2/4$ as $\theta\rightarrow 0$. The number of bound states increases rapidly at very small θ, suggesting that the number of bound states increases without limit, and that the energy $\pi^2/4$ is an accumulation point for such states. This behavior results from the fact that as $\theta\rightarrow 0$ these waveguides have an infinite amount of additional space, relative to a bent system of constant width.

III. CALCULATION OF BOUND-STATE ENERGIES

We used two separate methods to calculate the bound-state energies and wave functions for scalar fields inside the bent two-dimensional surfaces. The first was a relaxation method which has been extended to treat both the ground state and excited bound states of the system. The second method involved expanding the bound-state wave function in the center of the surface and on the legs, and then matching the wave function and its first derivative at the boundaries. We describe each of these techniques in this section.

A. Relaxation method for finding bound states

Here we will outline a relaxation method for obtaining the bound states for a bent waveguide. This involves finding a number of low-lying eigenvalues and eigenvectors of some Hamiltonian operators $\mathcal{H}$, using a method developed by one of us.[18] As this method is a generalization of the power method used to find the lowest eigenvalue of an operator, we first review this process.

Consider the differential equation

$$-\frac{\partial\psi}{\partial t}=\mathcal{H}\psi\ , \tag{5}$$

where the operator $\mathcal{H}$ has eigenvectors φ_k with eigenvalues ϵ_k. If we take an initial state $\psi^{(0)}$ to be a vector with randomly chosen elements, then in general

$$\psi^{(0)}=\sum_k a_k^{(0)}\varphi_k\ , \tag{6}$$

with all $a_k^{(0)}\neq 0$. The solution of Eq. (5) can immediately be written as

$$\psi(t)=\sum_k a_k^{(0)}e^{-\epsilon_k t}\varphi_k\ .$$

If Eq. (5) is discretized, then, using the index i for the ith time step and solving for $\psi^{(i+1)}$,

$$\psi^{(i+1)}=\psi^{(i)}-\Delta t\mathcal{H}\psi^{(i)}\ . \tag{7}$$

Equation (7) will converge provided the time step Δt satisfies the relation

$$|1-\Delta t\epsilon_{\max}|<|1-\Delta t\epsilon_0|\ , \tag{8}$$

where $\epsilon_{\max}$ (ϵ_0) is the largest (smallest) eigenvalue for the discretized Hamiltonian. If $\epsilon_{\max}>0$ and $\epsilon_{\max}\gg\epsilon_0$, then

$$\Delta t<\frac{2}{\epsilon_{\max}}\ . \tag{9}$$

It is easy to find the largest eigenvalue $\epsilon_{\max}$. Starting with the random eigenfunction $\psi^{(0)}$ of Eq. (6), repeatedly operating with $\mathcal{H}$ and renormalizing effectively multiplies each eigenfunction φ_k by a factor proportional to its eigenvalue ϵ_k. Repeated applications of $\mathcal{H}$ and renormalization rapidly leaves the resulting wave function dominated by $\varphi_{\max}$, the eigenvector with the largest eigenvalue. From $\varphi_{\max}$ we determine $\epsilon_{\max}$, and then Eq. (9) gives an upper limit for the value of Δt to use to iterate Eq. (7).

The one additional parameter of interest is the rate of convergence η, determined by how fast the second-lowest eigenfunction φ_1 dies off relative to the lowest eigenfunction φ_0; η is given by

$$\eta=\frac{1-\Delta t\epsilon_1}{1-\Delta t\epsilon_0}\approx 1-2\Delta t(\epsilon_1-\epsilon_0)\ .$$

To speed up convergence, we choose the time step Δt to be as large as possible subject to the restriction of Eq. (8).

We now wish to extend this method to find the eigenvalue of $\mathcal{H}$ that is closest to some arbitrary λ. To do this we produce some operator $\mathcal{A}$ which has the same eigenvectors as $\mathcal{H}$, but which has a minimum eigenvalue $\alpha_k(\lambda)$ for some eigenvector φ_k. We can then use the relaxation method on the operator $\mathcal{A}$ to find φ_k, then φ_k will also be the eigenvector of $\mathcal{H}$ with its eigenvalue closest to λ. We repeat the iteration process as before with

$$\psi^{(i+1)}=\psi^{(i)}-\Delta t\mathcal{A}\psi^{(i)} , \tag{10}$$

with time step Δt satisfying

$$\Delta t<\frac{2}{\alpha_k+\alpha_{\max}} .$$

Choosing $\mathcal{A}$ to be a polynomial in $\mathcal{H}$ ensures they have the same eigenfunctions. For example, we might use the operator

$$\mathcal{A}=(\mathcal{H}-\lambda)^2 , \tag{11}$$

which has a local minimum at λ. However, we also wish to minimize $\alpha_{\max}$. We may do so by choosing a higher-order polynomial in $\mathcal{H}$, for example

$$\mathcal{A}=\frac{(\mathcal{H}-\lambda)^2(\mathcal{H}-\epsilon_{\max})^2}{\epsilon_{\max}^2} , \tag{12}$$

since $\mathcal{A}$ defined in Eq. (12) has a significantly smaller maximum value $\alpha_{\max}$ than Eq. (11). This results in much faster convergence since the convergence factor η for Eq. (12) has the value

$$\eta\approx 1-\frac{(\epsilon_{k+1}-\epsilon_k)^2}{16\epsilon_{\max}^2} .$$

We may generalize this to higher-order polynomials in $\mathcal{H}$. In Fig. 3, we show a plot of various polynomials in $\mathcal{H}$, demonstrating how rapidly we can reduce $\alpha_{\max}$, thereby increasing the convergence rate. The price we pay for more rapid convergence is that we must multiply by larger powers of $\mathcal{H}$. However, in our case $\mathcal{H}$ is an extremely sparse matrix, so this is relatively cheap. The advantage of this method is that we never diagonalize or invert $\mathcal{H}$.

We now apply this method to the problem at hand. We approximate the two-dimensional wave function with one evaluated on a discrete set of points. These points are on the interstices of a rectilinear mesh with sides parallel to the boundaries of the waveguide. In our calculation, the length of the arms of the waveguide were six times their width, and the mesh size was taken to be $\frac{1}{40}$ of the width. On this mesh we approximate the Hamiltonian with a discrete Laplacian. We then numerically solve Eq. (7), normalizing after each time step, until the energy approaches its asymptotic value, ϵ_0.

We find the next eigenvalue by choosing a polynomial in $\mathcal{H}$ with zeros equally spaced between λ and $\epsilon_{\max}$. In practice we choose a twelfth-order polynomial with six zeros. A small linear term is added to this polynomial to ensure that λ is an absolute minimum. We then choose a value of $\lambda>\epsilon_0$, and iterate Eq. (10); we increase λ until we leave the basin of attraction of ϵ_0 and instead asymptotically flow to ϵ_1. We may increase λ still further to find ϵ_2, etc. Once we have found an eigenvalue, it is simple to calculate it as a function of θ, since to find $\epsilon_n(\theta+\Delta\theta)$ we may use $\epsilon_n(\theta)$ as λ.

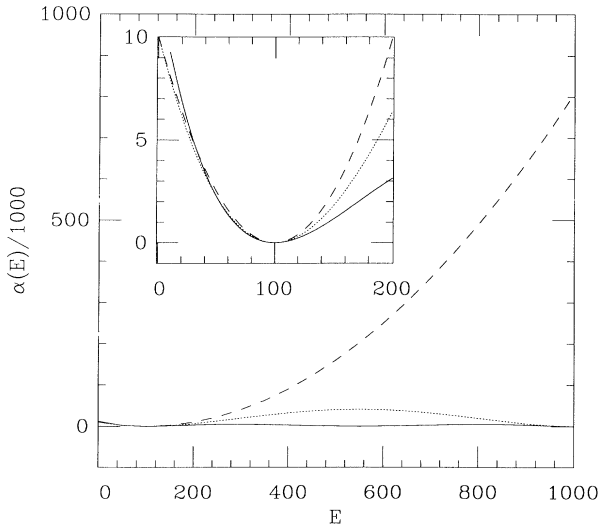

FIG. 3. Polynomical in $\mathcal{H}$ that can be used in the relaxation method to isolate the eigenvector of $\mathcal{H}$ with a given eigenvalue. For convenience, we assume a minimum value $\alpha(\lambda)=0$, and we search for an eigenvalue near $\lambda=100$. The dashed line is the function $\alpha(E)=(E-\lambda)^2$, the dotted line is $\alpha(E)=(E-\lambda)^2(E-\epsilon_{\max})^2/\epsilon_{\max}^2$, and the solid line is $\alpha(E)=(E-\lambda)^2(E-\epsilon_{\max}/2)^2(E-\epsilon_{\max})^2/\epsilon_{\max}^4$. Note the substantial decrease in the maximum value of the function $\alpha(E)$ by going to higher-order polynomials. Inset: the same functions plotted on a magnified scale near $\lambda=100$, showing the same parabolic behavior for each function near $E=\lambda$.

B. Series-expansion method

We have also used a series-expansion method to calculate the bound-state wave functions. This approximation is essentially that of Tang, Kleinman, and Karplus[19] and Eyring, Walter, and Kimball,[20] who used it to solve a simple model for chemical reactions which could be reduced to our bent waveguide problem. In this method we first note that the bound-state wave functions for the bent waveguide must be symmetric upon reflection across the diagonal (the dashed line in Fig. 4), since the Hamiltonian is symmetric upon reflection of the coordinates about the diagonal in the waveguide.[21] Thus we search for solutions on half the waveguide, with Neumann boundary conditions on the diagonal (vanishing of the normal derivative there). We divide the channel into (contiguous) regions labeled I and II in Fig. 4. Region I defines the straight right-hand section of the waveguide, defined by the relation $x\geq\cot(\theta/2)$, where θ is the opening angle of the waveguide. We expand the wave function $\psi_{\rm I}$ in Cartesian coordinates, where $\psi_{\rm I}(x,y)$ satisfies $(\nabla^2+k^2)\psi_{\rm I}=0$ with boundary conditions

$$\psi_{\rm I}(x,0)=\psi_{\rm I}(x,1)=0, \quad \psi_{\rm I}(x,y)\underset{x\to\infty}{\longrightarrow}0 . \tag{13}$$

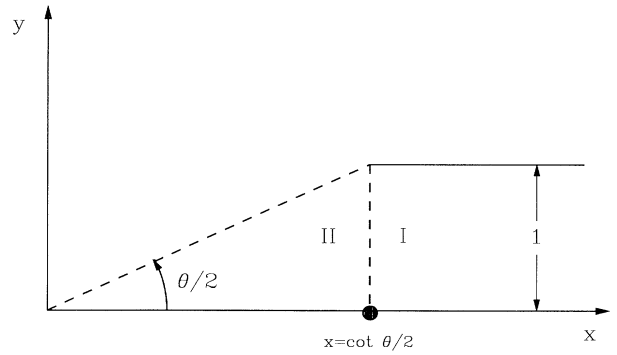

FIG. 4. A figure showing half of the bent waveguide of Fig. 2(a), divided into exterior section I and interior section II.

The final boundary condition in Eq. (13) is required by the confined nature of the bound-state wave function. Separation of variables in Cartesian coordinates then gives the series solution

$$\psi_{\rm I}(x,y)=\sum_{n=1}^{\infty} E_n \sin(n\pi y) e^{-\alpha_n x} , \tag{14}$$

where $\alpha_n=\sqrt{n^2\pi^2-k^2}$.

Region II is defined by $x\le\cot(\theta/2)$, $y\le x\tan(\theta/2)$. We expand the wave function in this region in two-dimensional polar coordinates (ρ,ϕ), since the boundary conditions are most easily expressed in these coordinates. In region II, the boundary conditions are

$$\begin{aligned} &\psi_{\rm II}(\rho,0)=0, \quad \left.\frac{\partial\psi_{\rm II}}{\partial\phi}\right|_{\phi=\theta/2}=0 \\ &\psi_{\rm II}(R,\theta/2)=0, \quad R\equiv\csc(\theta/2) . \end{aligned} \tag{15}$$

Full solution of the problem is obtained by matching the wave functions and normal derivatives at the boundary of regions I and II, i.e., $x=\cot(\theta/2)$, $0\le y\le 1$.

It is straightforward to show that the following wave functions satisfies the boundary conditions of Eq. (15) in this region:

$$\begin{aligned} &\psi_{\rm II}(\rho,\phi)=\sum_{j=1}^{\infty} B_j G_j(\rho,\phi) , \\ &G_j(\rho,\phi)=J_{\beta_j}(k\rho)\sin[\beta_j\phi] \\ &\qquad +\frac{J_{\beta_j}(kR)}{J_{\beta_{j+1}}(kR)} J_{\beta_{j+1}}(k\rho)\sin[\beta_{j+1}\phi] , \end{aligned} \tag{16}$$

where the J's are cylindrical Bessel functions and $\beta_j\equiv(2j-1)\pi/\theta$. The coefficients E_n and B_j are determined from the conditions that ψ and its derivative be continuous at the boundary between regions I and II, and that ψ be normalized.

To apply the continuity conditions for the wave functions $\psi_{\rm I}$ and $\psi_{\rm II}$ at the boundary between regions I and II, it is useful to expand the wave functions and normal derivative in a Fourier series, defining

$$\begin{aligned} &\tilde{G}_n(y)\equiv G_n(\rho,\phi)\Big|_{x=\cot(\theta/2)} , \\ &\tilde{H}_n(y)\equiv \left.\frac{\partial G_n}{\partial x}\right|_{x=\cot(\theta/2)} \\ &\qquad =\left[\frac{\partial G_n}{\partial\rho}\cos\phi-\frac{\partial G_n}{\partial\phi}\frac{\sin\phi}{\rho}\right]\Bigg|_{x=\cot(\theta/2)} . \end{aligned} \tag{17}$$

Then write

$$\tilde{G}_n(y)=\sum_m b_{nm}\sin(m\pi y) ,$$

$$\tilde{H}_n(y)=\sum_m d_{nm}\sin(m\pi y) .$$

The matching conditions for the wave functions and normal derivatives at the boundary

$$\psi_{\rm II}(x,y)\Big|_{x=\cot(\theta/2)}=\psi_{\rm I}(x,y)\Big|_{x=\cot(\theta/2)} ,$$

$$\left.\frac{\partial\psi_{\rm II}}{\partial x}\right|_{x=\cot(\theta/2)}=\left.\frac{\partial\psi_{\rm I}}{\partial x}\right|_{x=\cot(\theta/2)} ,$$

give the relation

$$\sum_{n=1}^{\infty}(d_{nm}+\alpha_m b_{nm})B_n=0 , \tag{18}$$

so defining the matrix

$$C_{nm}\equiv d_{nm}+\alpha_m b_{nm} , \tag{19}$$

which is a function only of k^2, a nontrivial solution to Eq. (18) exists only if $\det|C(k^2)|=0$.

We truncate the (infinite dimensional) expansion Eq. (18) at N terms, making C an $N\times N$ matrix, and search for values of k^2 for which $\det|C(k^2)|=0$. Having found the relevant values of k^2, the coefficients E_m and B_m can be found and we can reconstruct the wave functions ψ (and hence the electric and magnetic fields in the waveguide) for each bound state. In our calculations we have truncated our expansion at $N=4$. We find that both the bound-state energies and wave functions are stable and relatively accurate with this small number of expansion coefficients. As we want to calculate bound-state energies for very sharply bent waveguides (very small values of θ), the coefficients β_j of Eq. (16) become extremely large, so that we need to calculate cylindrical Bessel functions of very large order and small argument. To evaluate $J_\nu(x)$ in this calculation, we generally use the IMSL routine DBJS; however, we sometimes encounter cases where the VAX double precision routine DBJS returns a value of zero. In this case we substitute a cylindrical Bessel function algorithm from Ref. 22. We will show bound-state energies and expansion coefficients in Sec. V.

IV. EXPERIMENTAL MEASUREMENTS

To observe the lowest bound state in an electromagnetic waveguide bend for different bend angles, we con-

structed a simple realization of the variable-angle bend geometry shown in Fig. 2(a). With this system we can measure the microwave bound-state frequency as a function of bend angle θ between 60° and 120°. To search for multiple bound states, which are predicted to occur in bends with smaller interior angles, we also made a bend with a fixed internal angle ($\theta=22.5°$). The fixed-angle bend offers increased mechanical stability, which we found to be crucial in mapping out the electric- and magnetic-field distribution for each of the bound states.

For the variable-angle bend, parallel brass plates serve as the top and bottom of the bend structure. The plates are held apart by milled pairs of aluminum bars. The bars define the sides of the straight waveguide sections, and their thickness ($b=0.953$ cm) and length (20 cm) determine the height and length of the waveguides, respectively. The inner pairs of bars contact at the sharp inner tip of the waveguide bend. The outer pair of bars, machined to overlap, form the complementary angle at the outer point.

In an ideal structure with walls of infinite conductivity, propagating waves with frequencies below c/b ($=15.75$ GHz here) can only have a nonzero component of the electric field perpendicular to the large plates in order to satisfy the boundary conditions on those conducting surfaces.

During construction of the structure, aluminum parallels (1.905 cm wide and 0.94 cm thick) facilitate keeping the inner and outer sides of the waveguides parallel. The parallels give the waveguides a nominal width, $a=1.905$ cm, which implies a nominal TE_{01} cutoff frequency $f_{co}=c/2a=7.87$ GHz. The actual cutoff frequency can be determined experimentally by using a similar procedure to construct a rectangular cavity with the same nominal width and a relatively better-known length $l \gg a$, and then measuring the frequencies of the first few TE_{01n} modes, f_n. A linear fit to the data: $f_n^2=f_{co}^2+n^2(c/2l)^2$, gives $f_{co}=(7.780\pm0.015)$ GHz.

Since the bound-state frequencies are typically well below the cutoff frequency of the waveguide, it is impractical to send microwave power directly into the bend region through the straight waveguide sections. Instead we send the microwaves into the bend region through a 0.141 in. semirigid coaxial line that passes through a $\frac{9}{64}$-in. clearance hole in the top brass plate. The center conductor of the coax protrudes five millimeters beyond the outer conductor in order to radiate into the wave guide structure. We adjust the amount of coupling of the coax to the waveguide by varying the length of the protrusion that extends into the waveguide. With a Hewlett-Packard 8510B network analyzer we measure $R(f)$, the ratio of the microwave power reflected from the end of the coax to the incident power as a function of frequency. A bound state appears as a sharp decrease in reflected power, that is, as a resonant absorption of power, for microwave frequencies below the cutoff frequency. To determine the bound-state frequency, we decrease the coupling of the coax until (1) it is much less than critical coupling (when all incident power is absorbed at resonance), and (2) further decrease does not affect the resonant frequency or bandwidth of the resonance.

Once we can measure the resonant frequency, we can map out the field distribution for each resonance. The simplest two-dimensional mapping procedure is a technique which has been known for some time,[23] and which has been investigated in some detail by Sridhar.[24] In this method the resonance is perturbed with a small steel ball ($\frac{1}{8}$-in. diameter) located at a known position within the waveguide bend and then we measure the change in the resonant frequency of the mode as a function of position, $\Delta f(x,y)$. We locate the steel ball (with a precision of about 1 mm) on the vertices of a 0.5-cm two-dimensional grid with a small magnet, so that we do not need to disassemble the waveguide structure during the mapping procedure.

Since the radius r of the ball satisfies the inequality

$$\delta \ll r \ll \lambda , \tag{20}$$

where δ is the skin depth for the ball and λ is the microwave wavelength, the surface charges (or currents) effectively force the ac electric field (or magnetic induction) to be zero inside the ball, and the resulting induced electric and magnetic polarization of the ball can be calculated easily. For example, for fixed sources the presence of the ball in the unperturbed field, E_0, will lower the stored electric-field energy by $-\frac{1}{2}p_0E_0$, where the induced electric dipole moment is $p_0=4\pi r^3\varepsilon_0E_0$. The change in resonant frequency produced by the perturbation, $\Delta f=f_{pert}-f_0$, can be related simply to the time-averaged electric- and magnetic-field energy densities of the unperturbed resonance (u_{oe} and u_{om}, respectively) at the position of the ball:

$$\frac{\Delta f(x,y)}{f_0}=-\frac{4\pi r^3}{U_{tot}}[u_{oe}(x,y)-\tfrac{1}{2}u_{om}(x,y)] , \tag{21}$$

where U_{tot} is the total electromagnetic energy at resonance.

In a cavity at resonance, we expect comparable maximum values for u_{oe} and u_{om}, and so the maximum positive and negative frequency shifts for a given mode should be the same order of magnitude. Therefore, Eq. (21) differs from similar formulas found in Ref. 24, which asserts that the frequency shift is proportional to the electric-field energy density with a correction of a few percent due to the magnetic-field energy density. While Eq. (21) is certainly correct if the sources of the fields interacting with a small metal sphere are fixed, it is reasonable to ask if this assumption is realized in the experiment.

In this experiment the diameter of the sphere is 0.315 cm, and it rests on the bottom plate of the structure (the top plate is only 0.953 cm above the base plate), so the presence of the sphere will certainly affect the surface charge distribution and surface current-density distribution, especially on the bottom plate. In fact there is good evidence, in the form of the effect of the sphere on the Q factor of the resonance (discussed below), that the current sources are not fixed. Nevertheless, the positive frequency shifts that we measure are consistent with the values calculated by Eq. (21) with theoretical predictions for the electric- and magnetic-field energy density.

As discussed in Sec. V, however, our measured negative frequency shifts are about twice as large as predicted by Eq. (21). Therefore, we need to drop the assumption of fixed surface charge density on the inner surfaces of the waveguides; this greatly increases the difficulty of calculating the effect of the sphere on the stored electric energy. We want to calculate the change in electric-field energy caused by placing a conducting sphere on a conducting plate in the presence of a parallel sheet of charge. This problem is equivalent to calculating one half the change in electric energy produced by inserting two identical touching spheres into a uniform electric field (pointing along the symmetry axis) produced by fixed sources. To apply the calculation to the experiment, we still need to assume that the charges on the top plate of the waveguide structure are fixed, which is a much better approximation than assuming that the charges on both plates are fixed.

For two touching spheres, we can calculate the induced dipole moment in response to the electric field E_0 produced by two distant equal but opposite charges located on the symmetry axis by employing an infinite series of image charges inside each sphere.[25] The net dipole moment $p_{\rm net}$ of the two spheres is

$$p_{\rm net}=E_0(4\pi\varepsilon_0 r^3)4\left[\sum_{n=1}^{\infty}\frac{1}{n^3}\right]\approx 4.808\cdots p_0\ , \qquad (22)$$

where p_0 is the induced dipole moment of a single sphere of radius r in a uniform electric field E_0.

The change in the electric-field energy for one sphere on a conducting plate will be one half the change in energy for the two-sphere problem: $\frac{1}{4}p_{\rm net}E_0$. This model predicts that the frequency shift follows a form similar to Eq. (21), but with the electric-field energy density $u_{\rm oe}$ multiplied by a constant $2\zeta(3)=2.404\ldots$, where $\zeta(z)$ is the Riemann ζ function of argument z. We estimate that the error in assuming that the charges on the top plate are fixed is on the order of the attractive potential energy of the induced dipole moment, $p_{\rm net}=4.808p_0$ to its image on the top plate. This produces a correction to the change in electric-field energy of order

$$\Delta U_{\rm elec}\approx -\frac{2p_{\rm net}^2}{(2b)^3}=2(4.808)^2\left[\frac{r}{2b}\right]^3(\tfrac{1}{2}p_0E_0)\ ,$$

In our experiment ($b=6r$), the correction is roughly 5% of the change in the electric energy produced by an isolated sphere. Therefore a better estimate of the constant mentioned in the previous paragraph would be 2.46.

We have assumed that $\Delta f(x,y)\ll f_0$ and we have ignored the penetration of the fields into the sphere: since $\delta\ll r$ the correction to the stored magnetic-field energy produced by the penetrating field is small compared to the change in magnetic energy produced by the presence of the sphere, and the resulting Ohmic losses are small compared to Ohmic losses in the rest of the waveguide structure. Of course, these assumptions can be verified experimentally for a ball with a given radius. In our experiment the maximum frequency shift is always on the order of 2% of f_0 (always less than 0.1 GHz), and no perceptible change in the Q factor occurs during the mapping procedure, with one significant exception. When the ball approaches the inner point of the bend, the Q factor actually increases. The presence of the ball screens the local magnetic field, which reduces the magnitude of the local surface current density (and associated Ohmic losses) in the vicinity of the point.

Our mapping technique measures a combination of the electric- and magnetic-field strength that has no simple analog for the quantum bound state. We can generate a theoretical prediction for the quantity that is equivalent to Eq. (21):

$$\frac{\Delta f(x,y)}{f_0}=-\frac{4\pi r^3}{2ba^2}\left[c\,|\psi(x,y)|^2-\frac{1}{2k^2}\left[\left|\frac{\partial\psi(x,y)}{\partial x}\right|^2+\left|\frac{\partial\psi(x,y)}{\partial y}\right|^2\right]\right]\ , \qquad (23)$$

where we assume that the wave function ψ is normalized, and the constant $c\approx 2.46$ was derived from Eq. (22).

We can also compare the measured position of antinodes for the electric-field amplitude with theoretical predictions for antinodes of the bound-state wave function. Even though we do not directly measure the electric-field amplitude, since we are measuring the fields of effectively two-dimensional modes (the fields have no dependence on z), antinodes of E_z correspond to nodes of the transverse magnetic field, $H_t=[H_x^2+H_y^2]^{1/2}$ (the reverse is not always true, as antinodes of H_t do not necessarily coincide with nodes of E_z). Therefore, the positions of the ball that produce local minima in the resonant frequency of a mode also correspond to antinodes of the electric field for that mode, and positions that produce local maxima in the resonant frequency correspond to antinodes of the transverse magnetic-field strength. Note that positions where $\Delta f=0$ have no special significance as nodes or antinodes of the electric or magnetic field, except when both the electric- and magnetic-field amplitudes are small.

V. RESULTS AND CONCLUSIONS

In Fig. 5(a), we show the bound-state eigenvalues (divided by π^2) as a function of the interior bend angle θ of the waveguide. We show the first five bound states as a function of θ. The numerical eigenvalues and expansion coefficients E_j and B_j [from Eqs. (14) and (16)] are also listed in Table I, for selected angles θ. The eigenvalues are identical whether we use the series-expansion method or the relaxation method. First, note that all bound-state energies tend toward $\pi^2/4$ in the limit $\theta\rightarrow 0$, as we argued previously. Second, the number of bound states in-

creases rapidly with decreasing angle θ, for very sharply bent waveguides. We have previously argued that the number of bound states should increase without limit as θ goes to zero. For example, for bend angles $\theta > 27.5°$ there is only a single bound state; below this angle there are at least two bound states. A third bound state appears at $\theta \approx 18°$, followed by a fourth around 11° and a fifth at about 9°.

Figure 5(b) shows the experimental $R(f)$ for the $\theta = 22.5°$ bend with the lowest degree of coupling strength between coax and waveguide that allows both modes to appear in the same frequency sweep. The ground state appears as the prominent minimum in $R(f)$ close to the small-coupling resonant frequency, $f_{gs} = 5.666$ GHz [equivalent to a bound-state energy of $(0.530 \pm 0.002)\pi^2$, indicated by the leftmost arrow], and the first excited state is close to the low coupling resonant

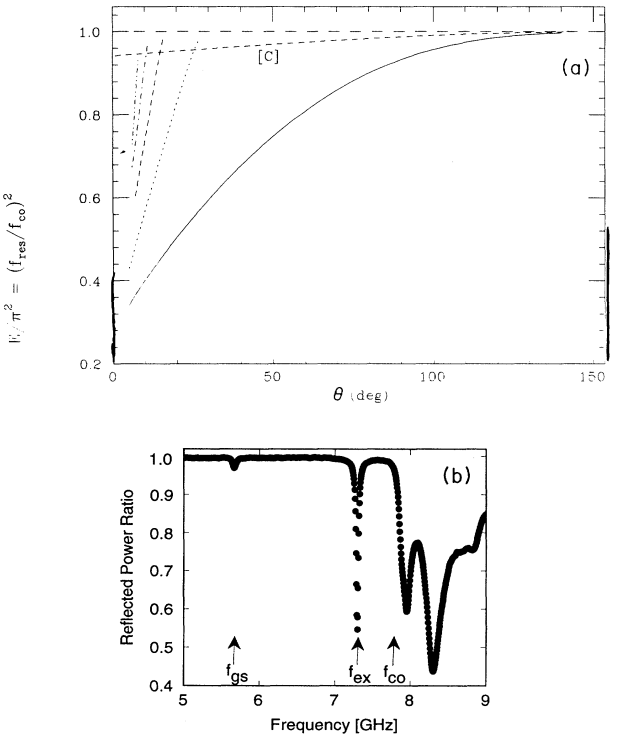

FIG. 5. (a) A figure showing bound-state energies for a sharply bent waveguide of the form of Fig. 2(a), as a function of the interior bend angle θ. R denotes the ratio of the square of the resonant frequency over the cutoff frequency $(f_{res}/f_{co})^2$. Solid curve: lowest-energy ($m = 1$) state; dotted curve: $m = 2$ state; dashed curve: $m = 3$ state; dot-dashed curve: $m = 4$ state; dash-dot-dot curve: $m = 5$ state. Dashed curve [C]: bound-state energy for a curved waveguide of constant width [the dashed curve in Fig. 2(a)]. (b) The experimentally measured ratio of reflected power to incident power as a function of incident frequency in GHz, for a waveguide with an interior bend angle $\theta = 22.5°$. The arrows denote the low-coupling resonant frequencies, f_{gs} and f_{ex} for the ground and first excited states, and the cutoff frequency f_{co} (i.e., the beginning of the continuum) for the straight waveguide sections.

TABLE I. Coefficients for the series expansion of the wave function. Columns are labeled by the bend angle θ with an index for the bound state(s), "1" standing for state of lowest energy.

	13°,1	13°,2	13°,3	22.5°,1	22.5°,2	45°,1	90°,1
$B(1)$	$0.100\,000 \times 10^{1}$	$0.100\,000 \times 10^{1}$	$0.100\,000 \times 10^{1}$	$0.100\,000 \times 10^{1}$	$0.100\,000 \times 10^{1}$	$0.100\,000 \times 10^{1}$	$0.100\,000 \times 10^{1}$
$B(2)$	$-0.945\,173 \times 10^{10}$	$0.806\,812 \times 10^{7}$	$-0.615\,725 \times 10^{5}$	$-0.605\,258 \times 10^{5}$	$0.425\,585 \times 10^{3}$	$-0.420\,098 \times 10^{2}$	$-0.193\,231 \times 10^{1}$
$B(3)$	$0.127\,621 \times 10^{32}$	$-0.275\,448 \times 10^{26}$	$0.214\,689 \times 10^{22}$	$0.165\,156 \times 10^{17}$	$-0.116\,034 \times 10^{13}$	$0.499\,793 \times 10^{7}$	$0.228\,772 \times 10^{3}$
$B(4)$	$-0.213\,323 \times 10^{58}$	$0.151\,168 \times 10^{50}$	$-0.161\,930 \times 10^{44}$	$-0.421\,962 \times 10^{31}$	$0.386\,812 \times 10^{25}$	$-0.226\,767 \times 10^{14}$	$-0.386\,063 \times 10^{6}$
$E(1)$	$0.816\,675 \times 10^{8}$	$-0.131\,907 \times 10^{7}$	$0.261\,310 \times 10^{4}$	$0.648\,070 \times 10^{4}$	$-0.337\,852 \times 10^{2}$	$0.136\,528 \times 10^{2}$	$0.935\,207 \times 10$
$E(2)$	$-0.622\,586 \times 10^{21}$	$0.149\,850 \times 10^{21}$	$-0.286\,573 \times 10^{20}$	$-0.133\,541 \times 10^{12}$	$0.314\,278 \times 10^{11}$	$-0.322\,613 \times 10^{5}$	$-0.109\,434 \times 10^{2}$
$E(3)$	$0.779\,752 \times 10^{33}$	$-0.332\,309 \times 10^{33}$	$0.121\,639 \times 10^{33}$	$0.936\,986 \times 10^{18}$	$-0.399\,084 \times 10^{18}$	$0.478\,282 \times 10^{8}$	$0.150\,001 \times 10^{3}$
$E(4)$	$-0.720\,765 \times 10^{45}$	$0.400\,951 \times 10^{45}$	$-0.196\,648 \times 10^{45}$	$-0.571\,315 \times 10^{25}$	$0.319\,168 \times 10^{25}$	$-0.697\,691 \times 10^{11}$	$-0.228\,898 \times 10^{4}$

frequency, $f_{ex}=7.305$ GHz [indicated by the central arrow, equivalent to a bound-state energy of $(0.882\pm0.004)\pi^2$]. Both resonances occur well below the measured cutoff frequency for the waveguide, $f_{co}=7.78$ GHz (equivalent to a quantum energy of π^2), indicated by the right arrow.

In our Sec. I, we discussed the role of both "bends" and "bulges" in producing bound states in bent systems. In the sharply bent systems under discussion here, the bound states arise from a combination of bend and bulge. In Fig. 2(a), we compare the sharply bent waveguide to a curved waveguide with no bulge (i.e., a sector of a circle with unit radius centered at the inner point of the waveguide). Because of the additional space present in the sharply bent waveguide, its bound-state energies will always be lower than the energy eigenvalues for the curved constant-width waveguide at the same angle. To demonstrate this we show the bound-state eigenvalue for the curved waveguide (the dashed curve marked [C] in Fig. 5(a)), and compare this with the binding energies for the sharp-cornered waveguide of the same opening angle.

By comparing the bound-state energy for the sharply bent and the curved waveguides, we can see the relative effects of the curvature and the "bulge" in producing binding. The curved waveguide of constant width has been studied by Sols and Macucci[7] and by Jackson.[26] The curved waveguide does not obtain a second bound state until the bend angle $\theta_c=5.047\pi$. The dominant effect on binding energy, and the number of bound states, comes from the additional space present in the corner of the sharply bent waveguide. The proliferation of bound states (which increase without limit) occurs because as $\theta\rightarrow 0$ this additional area becomes infinite.

As discussed in Sec. IV, we can measure and calculate the shift in frequency from insertion of a steel sphere into the waveguide. We display the experimental measurement of the field distribution of the ground state for $\theta=22.5°$ in Fig. 6(a) as a contour plot of $\Delta f(x,y)$. The underlying grid of data had a spacing of about $\frac{1}{4}$ of the waveguide width. Regions of negligible (less than 0.00005 GHz) frequency shift or negative frequency shift are unshaded. Positions with positive frequency shifts (regions of relatively large magnetic-field energy density) are shaded gray.

The labeled positions correspond to extrema of the measured frequency shift. The point marked "$E1$" represents the maximum measured negative frequency shift; it is the antinode of E_z [local minimum of $\Delta f(x,y)$], and points "$H1a$" and "$H1b$" are the antinodes of H_t [local maxima of $\Delta f(x,y)$]. Table II summarizes the locations of the extrema and the values of the frequency shift for those points, and the corresponding quantities calculated by the series-expansion method.

In Fig. (b), we plot the calculated value of the quantity given in Eq. (23) for the lowest bound state. In the inner band region, the experimental and theoretical plots resemble each other strongly, especially in the vicinity of point $E1$, the antinode of E_z (or the wave function). The pockets of largest positive frequency shift (large magnetic field energy) occur at the waveguide walls on either side of the antinode of E_z and around the inner tip of the bend; similar features appear in the calculated plot.

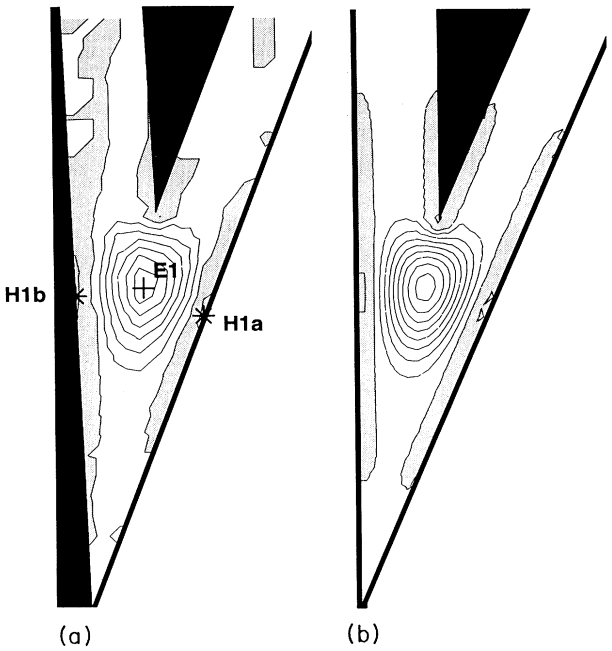

FIG. 6. (a) Experimentally measured contour plots of frequency shifts for lowest-frequency bound-state wave functions for a sharply bent waveguide with an interior angle $\theta=22.5°$. The frequency shift measured as a function of position for a small metal sphere inside the waveguide. Shaded areas denote regions of positive frequency shift (relatively large magnetic field energy density); unshaded areas signify negligible or negative frequency shift (negligible or relatively large electric-field energy density). Point $E1$ denotes the maximum negative-energy shift (antinode of E_z); points $H1a$ and $H1b$ denote points of the maximum positive-energy shift (antinodes of H_t). Numerical values of these quantities are given in Table II. (b) Calculations of the same quantity shown in (a), using Eq. (23).

Away from the bend region, especially down the straight waveguide sections and toward the outer tip of the bend, the resemblance of the two plots significantly decreases. In these areas, the measured frequency shifts become significantly smaller and quickly reach the experimental noise level, which accounts for the rough appearance of the contour line between the shaded and unshaded regions.

As seen in Fig. 6 and Table II, for the ground state the measured and calculated antinode positions agree within experimental uncertainty, which represents an overall ±0.1 cm (or $\pm0.05a$, in units of the waveguide width) uncertainty in the position of the ball relative to the structure. The experiment and calculation do not agree as well for the magnitude of the frequency shift values at the antinodes. The measured frequency shift at the antinode of E_z is only 75% of the calculated value. In contrast, the calculation gives a remarkably close estimate of the frequency shift at the antinodes of H_t. We have not tried to compare the experiment to the theory close to the inner point of the bend, where we expect a diverging

TABLE II. Experimental and theoretical antinodes of fields in a waveguide with 22.5° bend. Antinodes for ground state, shown in Fig. 6, and first excited state of Fig. 7. Letters refer to corresponding points shown on figures.

	Antinode type		Experiment		Calculation	
	Field	Location	Distance from outer point (a)$\pm$0.05a	Frequency shift (GHz), $\pm$1%	Distance from outer point (a)	Frequency shift (GHz)
Ground state (5.666 GHz)		(See Fig. 6)				
$E1$	E_z	Symmetry plane	4.18	−0.0692	4.217	−0.0925
$H1a$	H_t	Right wall	4.05	0.0133	4.072	0.0133
$H1b$	H_t	Left wall	4.05	0.0129	4.072	0.0133
Excited state (7.305 GHz)		(See Fig. 7)				
$E2$	E_z	Symmetry plane	3.27	−0.0969	3.257	−0.1220
$E3$	E_z	Symmetry plane	4.70	−0.0426	4.716	−0.0544
$H2$	H_t	Symmetry plane	4.13	0.0094	4.072	0.0094
$H3a$	H_t	Right wall	3.04	0.0161	3.134	0.0177
$H3b$	H_t	Left wall	3.14	0.0158	3.134	0.0177
$H4a$	H_t	Right wall	4.78	0.0053	4.815	0.0057
$H4b$	H_t	Left wall	4.88	0.005	4.815	0.0057

transverse magnetic-field energy density. In fact, we do measure a positive frequency shift for sphere positions close to the inner point; however, the region of the divergence must be localized enough that, as averaged over the volume of the perturbing sphere, the resulting positive frequency shift is not even as large as it is for the positions on the side walls that are close to the antinode of the electric field.

In Fig. 7, we show contour plots of the frequency shift for the first excited state; in Fig. 7(a), we show the experimental results (the mode at 7.305 GHz) and in Fig. 7(b) the calculation. Once again we find good overall agreement between calculations and measurement in the bend region. The major feature is the prominent antinode of E_z on the symmetry plane, which is labeled as "$E2$." Another antinode of E_z, labeled "$E3$" is closer to the inner point and smaller in magnitude. Between these points on the symmetry plane, we find an antinode of H_t marked "$H2$". On the side walls, additional antinodes of H_t seem to be associated with the nearby antinodes of E_z.

We summarize the positions and frequency shift values for the excited state in Table II. The measured and calculated positions of the electric-field antinodes agree within experimental error, but the measured frequency shifts at those points are again about 75–80 % of the calculated values. We measure the ratio of the shifts at the two antinodes as 2.27$\pm$0.03, which compares favorably with the calculated ratio of 2.24.

The theoretical calculation accurately predicts the position of the antinode of H_t located on the symmetry plane ("$H2$"), and also gives the measured frequency shift. The experiment and the calculation differ more significantly for the antinodes located on the outer walls; the positions agree fairly well (not as well as for the other antinodes) and the frequency shifts differ by about 10–12 %.

For both pairs of antinode positions on the walls, the measured values share two similar asymmetries: (1) the antinodes on the right wall seem to be about 0.10a closer to the outer point than the corresponding antinodes on the left wall, and (2) the frequency shifts are a few percent greater for the antinodes on the right wall. This difference probably represents the degree of asymmetry in the original construction of the structure. If there is a

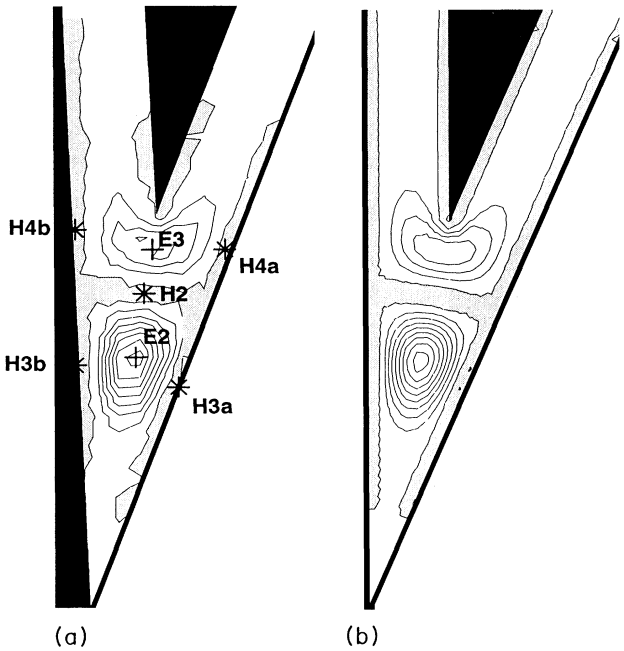

FIG. 7. Experimentally measured contour plots for the frequency shift for the first excited state of a bent waveguide with an interior angle θ=22.5°. The notation is that of Fig. 6. Points $E2$ and $E3$ denote maximum measured negative frequency shifts; points $H2$, $H3a$, $H3b$, $H4a$, and $H4b$ represent local maxima in the frequency shifts. (b) Calculations of the frequency shift for the same quantity shown in (a).

systematic error due to the asymmetry in the current experiment, it is slightly greater than the random error, and so it is probably not productive to try to greatly improve the sensitivity of the measurement without also improving the precision of the construction of the structure.

Overall, the measured positions of antinodes of E_z and H_t match the calculated values quite well. The calculations for the positive frequency shift values at antinodes of the transverse magnetic field are often surprisingly close to the experimentally measured values. We consistently measured negative frequency shifts that are about 75–80 % of the calculated values.

In Fig. 8, we show equal amplitude contour plots of calculations for the amplitude of the wave function, for $\theta=13°$, where there are three bound states. The lowest-energy state has a single maximum along the diagonal, roughly 70% of the way along the diagonal. The first excited state has a node in the frequency shift which corresponds quite closely to the maximum of the corresponding quantity in the ground state. If we define the sign of the wave function to be positive near the center of the waveguide, then the second bound-state wave function would have negative values along the "arms" of the waveguide, indicated by the shaded regions of the contour plot. The qualitative conditions for the third bound state in the 13° waveguide are identical, with this state having two nodes where the wave function vanishes.

In conclusion, we have shown how multiple confined states arise in sharply bent waveguide systems. Both bends and bulges in such systems produce effective attraction and hence binding. For the sharply bent waveguide shown in Fig. 2(a), the number of bound states increases without limit as the internal angle $\theta\rightarrow 0$. Furthermore, the energy of each of these states approaches $\pi^2/4$ in this limit, while the continuum begins at π^2. We demonstrated this by calculating the number of bound states and their energies as a function of θ. Two different methods of calculation, a relaxation method and a series-expansion method, give agreement on both the bound-state energies and electric field in such waveguides.

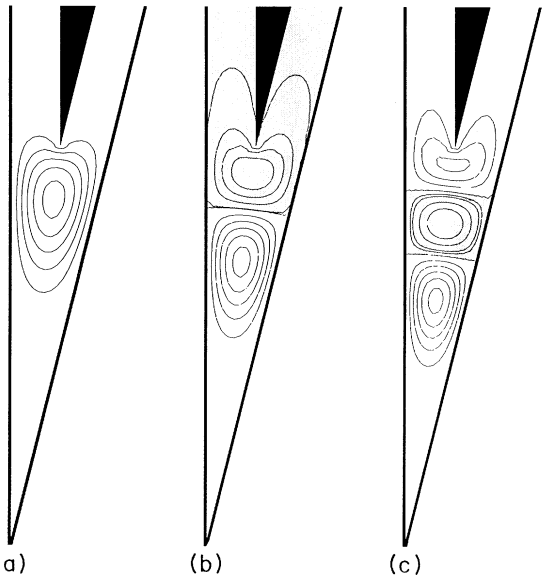

FIG. 8. A figure showing calculated contour plots for the wave-function amplitude of the three bound states for a bent waveguide with $\theta=13°$. (a) Ground state; (b) first excited state; (c) second excited state. Shaded regions denote negative values for the wave function; unshaded regions are positive values of the wave function.

Waveguides of this type were constructed, and the location of the confined states was experimentally demonstrated by measuring the ratio of reflected to incident power $R(f)$ as a function of frequency f for microwaves. The bound state appeared at that frequency where a sharp minimum in $R(f)$ was observed. The field distributions inside these waveguides were measured by moving a small metal sphere inside the waveguide and observing the shift in resonant frequency as a function of the position of the sphere. Although this process measures a combination of the E_z and H_t fields, the maximum and minimum frequency shifts correspond to antinodes of H_t and E_z, respectively.

We also derived a simple formula which related the resonant frequency shift to the electric- and magnetic-field densities in the waveguide. Qualitatively we obtained good agreement between theory and measurements. Quantitatively, we found very good agreement between theoretical predictions of the maximum frequency shifts (antinodes in H_t); however, theoretical predictions of the minimum frequency shifts overpredicted experimental results by 25–35 %.

The presence of confined electric and magnetic fields inside bent waveguide structures is not in itself particularly interesting. In most waveguides the practical interest is in the transmission and reflection well above the cutoff frequency, and the presence of confined states below cutoff frequency will have an influence on transmission properties of states above cutoff. Perhaps the most interesting thing about such states in bent waveguides is that they do not seem to have been predicted or measured before recently, despite decades of research on such systems.

The generality of the prediction of bound states in bent hollow waveguides suggest the possibility of finding similar states in other classes of waveguides. For example, although the boundary conditions are different, a bound state located at a bend in a dielectric waveguide would be more accessible to experimentation.

Because of the direct relation between scalar fields in curved surfaces in two dimensions, and electric fields in the rectangular waveguides constructed by translating the surface into the third direction (see the discussion of this point in Sec. I), electrons moving in curved quantum wires will also have bound states whenever a constant-width system has a bend. Similar bound states may have already been observed in experiments that observed a pair of resonant transmission peaks, for energies below the lowest propagating band through a quantum wire with two right-angle bends.[27] The presence of a bound electron at a bend in such a system can affect the flow of current, since it alters the local potential in the vicinity of

the bend. If the binding energy is small, then the hopping of electrons into and out of the bound state (due to thermal fluctuations) will introduce a dichotomic noise into the current. In addition, if the quantum wire is sufficiently short, such bound states can act as "impurity sites," through which electrons can resonantly tunnel.

As our investigations have focused on mapping out such states in waveguides, direct measurements of such bound-electron states in quantum wires have not been carried out. It would be extremely interesting to measure such states and compare or contrast them to the corresponding states in bent waveguides. In addition, a calculation of the transport of energetic electrons past a bound electron in a bent quantum wire could then be compared with experiment.

One additional property which could be measured in bent waveguides is the adiabatic relation which suggests that bends and constrictions in a waveguide could be correlated in such a way as to produce a reflectionless waveguide, at least over some range of frequencies.

ACKNOWLEDGMENTS

The authors wish to thank R. L. Jaffe for interesting conversations about the properties of these systems, and about results he and J. Goldstone had derived. Two of the authors (J.T.L. and D.P.M.) thank Scott Oser for assistance with calculations of bound state energies. The work in this paper was supported in part by the NSF under Contract Nos. NSF-PHY91-08036, NSF-DMR-9020816, and NSF-DMR-9113911. One of the authors (J.P.C.) acknowledges support from the Alfred P. Sloan Foundation.

[1]See, e.g., L. Lewin, *Theory of Waveguides* (Newnes-Butterworth, London, 1975).
[2]P. Exner and P. Seba, J. Math. Phys. **30**, 2574 (1989).
[3]P. Exner, Phys. Lett. A **141**, 213 (1989).
[4]M. L. Roukes, A. Scherer, S. J. Allen, Jr., H. G. Craighead, R. M. Ruthern, E. D. Beebe, and J. P. Harbison, Phys. Rev. **59**, 3011 (1988).
[5]G. Timp, H. U. Baranger, P. deVegvar, J. E. Cunningham, R. E. Howard, R. Behringer, and P. M. Mankiewich, Phys. Rev. Lett. **60**, 2081 (1988).
[6]F. M. Peeters, Superlatt. Microstruct. **6**, 217 (1989).
[7]F. Sols and M. Macucci, Phys. Rev. B **41**, 11 887 (1990).
[8]J. Carini, J. T. Londergan, Kieran Mullen, and D. P. Murdock, Phys. Rev. B **46**, 15 538 (1992).
[9]J. Goldstone and R. L. Jaffe, Phys. Rev. B **45**, 14 100 (1992).
[10]F. Lenz, J. T. Londergan, E. J. Moniz, R. Rosenfelder, M. Stingl, and K. Yazaki, Ann. Phys. **170**, 65 (1986).
[11]R. L. Schult, D. G. Ravenhall, and H. W. Wyld, Phys. Rev. B **39**, 5476 (1989).
[12]G. Dunne and R. J. Jaffe (unpublished).
[13]H. U. Baranger, A. D. Stone, and D. P. Di Vicenzo, Phys. Rev. B **37**, 6521 (1988).
[14]Mark Reed, Sci. Am. **268**, 118 (1993).
[15]Y. Aharonov and D. Bohm, Phys. Rev. **115**, 485 (1959).
[16]R. L. Jaffe (private communication).
[17]Y. Avishai, D. Bessis, B. G. Giraud, and G. Mantica, Phys. Rev. B **44**, 8028 (1991).
[18]Kieran Mullen, J. Math. Phys. (to be published).
[19]K. T. Tang, B. Kleinman, and M. Karplus, J. Chem. Phys. **50**, 1119 (1969).
[20]H. Eyring, J. Walter, and G. Kimball, *Quantum Chemistry* (Wiley, New York, 1944).
[21]The symmetry of the Hamiltonian would also allow wave functions antisymmetric upon reflection across the diagonal. However, for such wave functions there are no nontrivial solutions obeying the boundary conditions (wave functions which vanish on the top, bottom, and diagonal of the half waveguide).
[22]J. Spanier and K. Oldham, *An Atlas of Functions* (Hemisphere, New York, 1987), pp. 527–529.
[23]L. C. Maier and J. C. Slater, J. Appl. Phys. **23**, 68 (1954); J. C. Amato and H. Herrmann, Rev. Sci. Instrum. **56**, 696 (1985).
[24]S. Sridhar, Phys. Rev. Lett. **67**, 785 (1991); S. Sridhar and E. J. Heller, Phys. Rev. A **46**, R1728 (1992).
[25]See J. D. Jackson, *Classical Electrodynamics,* 2nd ed. (Wiley, New York, 1975), Chap. 2.
[26]A. D. Jackson (private communication).
[27]W. Yindeepol, A. Chin, A. Weisshaar, S. M. Goodnick, J. C. Wu, and M. N. Wybourne, in *Nanostructures and Mesoscopic Systems,* edited by W. P. Kirk and M. A. Reed (Academic, Boston, 1992), pp. 139–149.

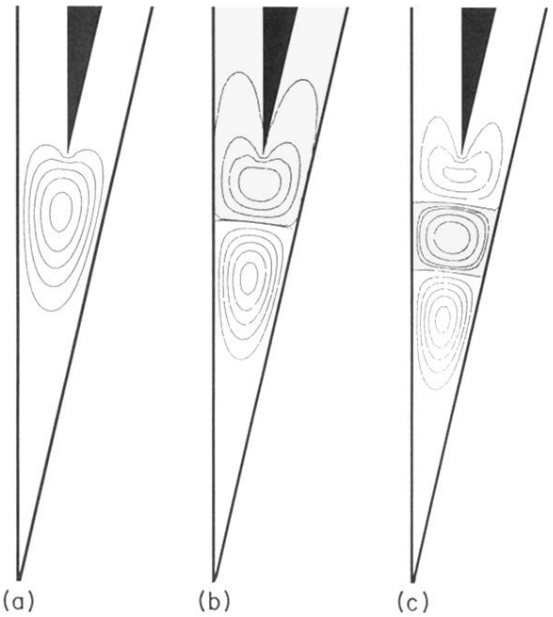

FIG. 8. A figure showing calculated contour plots for the wave-function amplitude of the three bound states for a bent waveguide with $\theta = 13°$. (a) Ground state; (b) first excited state; (c) second excited state. Shaded regions denote negative values for the wave function; unshaded regions are positive values of the wave function.